A new European coastal flood database for low-medium intensity events

Marine Le Gal[1,2], Tomás Fernández-Montblanc[3], Enrico Duo[1,2], Juan Montes Perez[1,3], Paulo Cabrita[1], Paola Souto Ceccon[1,2], Véra Gastal[4], Paolo Ciavola[1,2], and Clara Armaroli[5]

[1]Department of Physics and Earth Sciences, Università degli Studi di Ferrara, Via Saragat 1, Ferrara, 44122, Italy.
[2]Consorzio Futuro in Ricerca, Via Giuseppe Saragat, 1, Ferrara, 44122, Italy.
[3]Earth Sciences Department, University of Cadiz INMAR, Avda. República Saharaui s/n, Puerto Real, 11510, Cadiz, Spain.
[4]Collecte Localisation Satellite (CLS),11 rue Hermes, 31520, Ramonville st Agne, France
[5] Department of Biological, Geological and Environmental Sciences (BIGeA), University of Bologna Alma Mater Studiorum, 40126 Bologna, Italy

Correspondence: Marine Le Gal: marine.legal@unife.it

Abstract. Coastal flooding is recognized as one of the most devastating natural disasters, resulting in significant economic losses. Therefore, hazard assessment is crucial to support preparedness and response to such disasters. Toward this, flood map databases and catalogues are essential for the analysis of flood scenarios, and furthermore can be integrated into disaster risk reduction studies. In this study and in the context of the ECFAS project (GA 101004211), which aimed to propose a European

5 Copernicus Coastal Flood Awareness System, a catalogue of flood maps was produced. The flood maps were generated from flood models developed with LISFLOOD-FP for defined coastal sectors along the entire European coastline. For each coastal sector, fifteen synthetic scenarios were defined focusing on high-frequency events specific to the local area. These scenarios were constructed based on three distinct storm durations and five different Total Water Level (TWL) peaks incorporating tide, mean sea level, surge and wave set-up components. The flood model method was extensively validated against twelve test

10 cases for which observed data were collated using satellite-derived flood maps and in situ flood markers. Half of the test-cases well represented the flooding with hit scores higher than 80 %. The synthetic scenario approach was assessed by comparing flood maps from real events and their closest identified scenarios, producing a good agreement and global skill scores higher than 70 %. Using the catalogue, flood scenarios across Europe were assessed, and the biggest flooding occurred in well-known low-lying areas. In addition, different sensitivities to the increase of the duration and TWL peak were noted. The storm duration

15 impacts a few limited flood prone areas such as the Dutch coast for which the flooded area increases more than twice between a 12h and 36h storm scenarios. The influence of the TWL peak is more global, especially along the Mediterranean coast for which the relative difference between a 2- and 20-year return period storm is around 80 %. Finally, at a European scale, the expansion of flood areas in relation to increases in TWL (Total Water Level) peaks demonstrated both positive and negative correlations with the presence of urban and wetland areas, respectively. This observation supports the concept of storm flood

20 mitigation by wetlands.

1   Introduction

Flood hazard and risk are subjects of high concern due to the destruction and high cost caused by flooding. In the United States, 8 of the 10 most costly weather and climate disasters between 1980 and 2010 were floods and extensive efforts have been made to assess flood hazard, gathering coastal, fluvial and pluvial risk, for present and future climate scenarios (Bates et al., 2021). In
25 Europe, between 1998 and 2009, flooding, mainly fluvial, was the most recorded natural disaster resulting in the largest overall economic losses (European Environment Agency, 2010). The role played by Early Warning Systems (EWS) is thus critical to support preparedness and response after such disasters. Since 2012, as part of the Copernicus Emergency Management Services, the European Flood Awareness System (EFAS) has become operational, predicting fluvial flood magnitude for the major rivers of the continent (Smith et al., 2016; Dottori et al., 2017). The daily streamflow forecast is connected to a database
30 of flood hazard maps (Dottori et al., 2022) such that, using a rapid mapping process, event-based rapid risk assessments can be produced and provided to stakeholders and decision makers. The advantages of such a system are multiple with, at local scale, a joint evaluation of fluvial risks, and, at European scale, shared information for prioritising and coordinating support across the national emergency services (Dottori et al., 2017).

No such EWS currently exists for coastal flooding at European scale, despite coastlines coming under growing pressure due to
35 the increasing coastal population and infrastructures along with exposure to extreme events (Merkens et al., 2016; Calafat et al., 2022; Portner et al., 2022). It is in this context that the H2020 ECFAS project (A proof of concept for the implementation of a European Copernicus Coastal Flood Awareness System, GA n° 101004211, https://www.ecfas.eu/) aimed to suggest tools for European coastal risk EWS. Similar to the EFAS system, the ECFAS concept relies on a forecast of coastal extreme water level (Irazoqui Apecechea et al., 2023) that is connected to a flood map catalogue, allowing for rapid flood risk assessment. Indeed,
40 a catalogue gathers maps representing different possible flood scenarios affecting a coastal area that could be quickly retrieved without the necessity to run operational models. As these flood scenarios are defined by the nearshore forcing condition affecting the area, it is then assumed that every real flood scenario could be represented by the catalogue's equivalent with the forcing conditions that are the most similar to the real one. Coastal flood hazard assessment is usually performed at a local scale, and only a few flood databases targeting large and continent-wide scales exist (Barnard et al., 2014; Hinkel et al., 2014;
45 Mokrech et al., 2015; Forzieri et al., 2016; Muis et al., 2016; Vousdoukas et al., 2016). Mokrech et al. (2015) built the Coastal Fluvial Flood (CFFlood) model from the global Dynamic Interactive Vulnerability Assessment database (DIVA, Vafeidis et al. 2008) using coastal flood zones generated statically, such as with the bathtub method, for 1, 10, 100 and 1000 year events. Muis et al. (2016) constructed the GTSR database, also using a static method, to estimate the flood hazard for a 100 year extreme sea level scenario. Similar to the GTSR database, the TUD database was developed for the "Risk analysis of infrastructure networks in response to extreme weather" (RAIN) project focusing on return levels of 10, 30, 100 and 200 years (Groenemeijer et al.,
50 2016; Paprotny et al., 2016). It is only with the work of Vousdoukas et al. (2016) that a coastal flood hazard database was generated using a flood dynamic model to estimate the flood extent, hereafter referred to as the JRC database. This database was developed using the LISFLOOD-FP model (Bates and De Roo, 2000; Bates et al., 2010) to simulate the flood propagation for a 100 year return level scenario. While some of the databases were validated by comparisons with observed data at local

scale, such as during the 2010 storm Xynthia at La Faute-sur-Mer (Vousdoukas et al., 2016), Paprotny et al. (2019) assessed the performance of the GTSR, JRC and TUD databases at large scale by comparing them to reference maps such as official national study maps, published research maps and an observed flood extent map. In their work, they highlighted a need for better analysis of the model's accuracy to be shared with stakeholders, and concluded that there was a low performance of the statically generated databases, as also pointed out by Bates et al. (2005); Seenath et al. (2016); Vousdoukas et al. (2016) and Gallien et al. (2018).

In light of the above, there is a lack of European coastal flood hazard assessment using more accurate dynamic methods with a robust validation process. In addition, the existing databases focused on high return level events. However, low return level - frequent events could be of interest to the stakeholders in EWS (Alves et al., 2022). In the frame of the ECFAS project, a new database of coastal flood maps was generated to assess the flood hazard at European scale for small-medium return events, hereafter referred to as the ECFAS flood map catalogue. While the previous flood databases rely on the characterisation of the forcing based only on the water return levels, the present analysis additionally integrates the storm duration, as recommended by Wahl et al. (2011), leading to 15 storm scenarios forcing the models. The objectives of the present paper are twofold: first, to present the ECFAS flood catalogue alongside the methodology used to produce it, as well as the validation of the modelling method through the simulation of twelve test cases, the assessment of the catalogue capacity to represent real events and its limitations; second, to assess the flood hazard patterns and sensitivity to the different scenarios across Europe. To go further, and as an application of the catalogue use, connections between the flood sensitivities and land use and coverage data in Europe were investigated.

2 Data sets

2.1 Topography

The Digital Elevation Model (DEM) COP-EEA-DEM-10 which is part of the Copernicus DEM products (European Space Agency and Airbus, 2022) was used as topography data. The horizontal spatial resolution is $\sim 10\ m$ with an absolute vertical accuracy lower than 4m. The associated water body mask (European Space Agency and Airbus, 2022) was used to extract the coastal water extent and to identify the coastline. This data was used to build the model grid and the boundary condition positions of the flood model.

2.2 LU/LC data

The EEA LU/LC Coastal Zone layer 2018 (CZ layer, Innerbichler et al. 2021) which is part of the Copernicus Land Monitoring Service was used to define the friction parameter. Innerbichler et al. (2021) derived their classification from Very High Resolution (VHR) satellite data and other available EO data, leading to 71 classes. The CZ layer was quality checked in the framework of the ECFAS project in order to produce a coastal dataset (Ieronymidi and Grigoriadis, 2022).

2.3   Total water level data

Total Water Levels (TWLs) at the coast include mean sea level, tides, atmospheric surges, wave set-up and swash (Melet et al., 2018). In the present work, the TWLs were extracted from the 10-year ECFAS combined hindcast (Melet et al., 2021) covering the time window 2010 - 2019. This hindcast relied on a linear addition of the different components. The tide and mean sea level were selected from FES2014 (Lyard et al., 2021) and Copernicus Marine high-resolution global ocean reanalysis GLORYS12 (Lellouche et al., 2021), respectively. The storm surge component was obtained using an upgraded version of the ANYEU-SSL ocean model (Fernández-Montblanc et al., 2020): the grid resolution was increased to $2.5\ km$ at the coastline and the atmospheric forcing was upgraded to ERA 5 global reanalysis (Hersbach et al., 2020). For the ECFAS combined hindcast, the swash component was discarded and the wave set-up η_{wsu} was approximated by the generic formulation derived by Holman and Sallenger (1985) and recommended by U.S. Army Corps of Engineers (2002):

$$\eta_{wsu} = 0.2 \times H_s,\tag{1}$$

where H_s is the significant wave height. For the ECFAS hindcast, H_s were taken from the Copernicus Marine Environment Monitoring Service (CMEMS) wave regional hindcast. Parameterising the wave set-up is common practice (Dodet et al., 2019) as an accurate representation of the nearshore wave components needs high resolution wave models that are not always available, especially at the large scales targeted in this work. So this approximation is considered sufficient in the present work. When the TWL time-series were not included into the ECFAS hindcast time window, such as during 2020, the relevant ocean and wave models from the CMEMS database were used (Clementi et al., 2021; Korres et al., 2021).

2.4   Test cases and observed data

In the present work, twelve test cases were identified across Europe from the storm database of Souto Ceccon et al. (2022) for validation purposes (Table 1 and Figure 1).

These test cases represent a large variety of coastal morphologies and oceanographic conditions (tidal range, storm surge level and wave energy) covering storms that occurred between 2010 and 2020 throughout Europe. This list gathers eight events covering twelve sites. Among the major events in the list, there are test cases covering the Xynthia storm (2010) that hit La Faute-Sur-Mer (France), the Gloria storm (2020) that hit the Mediterranean Spanish coast, and the Xaver storm (2013) that hit Norfolk (UK).

Two types of observed data were retrieved for the validation analysis: flood extension derived from satellite images as well as in-situ observations.

2.4.1   Satellite-based flood map

Flood mapping of historical events is highly dependent on the availability and quality of archived satellite images. The most relevant acquisitions in terms of timing with regards to the event, type of image, resolution and acquisition conditions were selected to detect flooded areas. The satellite derived flood extents were generated by differentiating the visible water surfaces
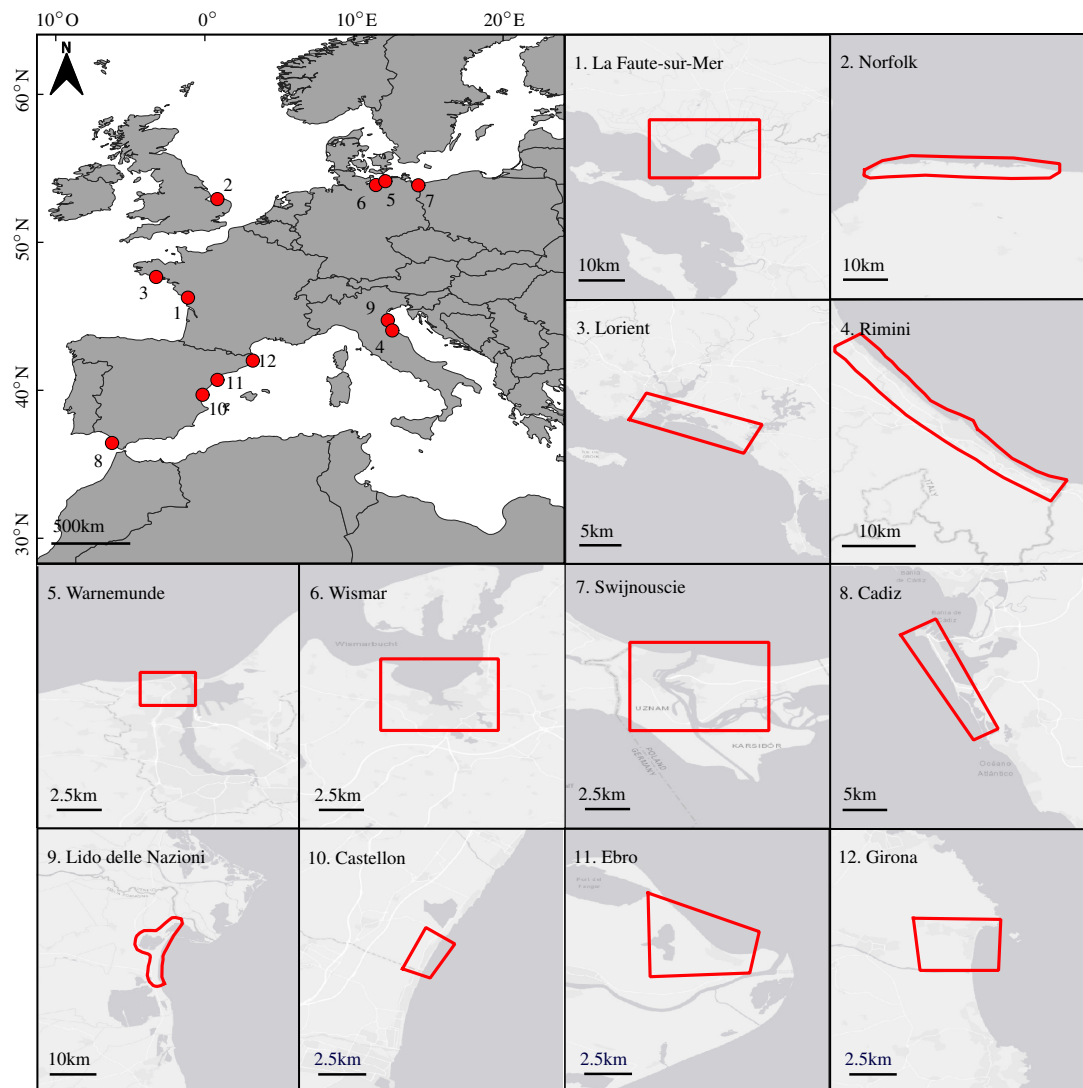
Figure 1. Location and area of interest of each test case extracted from the extreme event ECFAS database (Souto Ceccon et al., 2022) considered for the validation of the flood method. For details of the test cases, refer to Table 1

	Site	Event	Year	Satellite-based flood maps - time lapse between the event and post-event images acquisition [d]	Local flood markers - number of flood markers available
1.	La Faute-sur-Mer (FR)	Xynthia	2010	7	7
2.	Norfolk (UK)	Xaver	2013	0-6	13
3.	Lorient (FR)	no name	2014	2	7
4.	Rimini (IT)	Saint-Agatha	2015	5	8
5.	Warnemunde (DE)			2	NA
6.	Wismar (DE)	Axel	2017	2	4
7.	Swinoujscie (PL)			3	NA
8.	Cadiz (ES)	Emma	2018	NA	17
9.	Lido delle Nazioni (IT)	Vaia	2018	0	2
10.	Castellon (ES)			1	2
11.	Ebro (ES)	Gloria	2020	1	3
12.	Girona (ES)			2-4	13

Table 1. List of the test cases considered from the ECFAS extreme event database for the validation of the flood method and for which observed data were gathered. NA means not available sources and/or identifiable flood markers.

between the pre-event image used as reference and the post-event image. Water surfaces were mostly extracted using an automated workflow and manually refined if needed. In the case of RADAR images, the discrimination between water and non-water surfaces relied on the backscatter coefficient value: water surfaces typically hold low backscattering values as they are usually smooth and flat, reflecting the RADAR pulse away from the spacecraft. In the case of optical images, water was
120 extracted using the well-known Modified Normalised Difference Water Index (Xu, 2006), for images with a Short Wave InfraRed band (Copernicus Sentinel-2, Landsat missions, SPOT-5). Other optical images, mainly Very High Resolution (VHR) images, were analysed using a manual approach. The satellite images are acquired in the aftermath of an event, the time lapse between their acquisition and the events considered in the test cases are indicated in Table 1.

2.4.2 In situ flood markers

125 The in situ flood markers were retrieved by analysing the sources of information collected by Souto Ceccon et al. (2022), including, among others, videos, news or technical reports. Focusing in the areas of interest (Figure 1), the flood markers were precisely geolocalised and described by reviewing those already identified by other reports or scientific papers, or by thoroughly analysing pictures and/or videos with visible flood. The collected flood markers indicate flooded points or flood extension limits. In the present work, only flood markers that were precisely geolocated were used. The number of flood
130 markers per test case is indicated in Table 1.

3 Methods

3.1 Flood modelling approach

The flood modelling of this study was performed with the widely used LISFLOOD-FP model (Bates and De Roo, 2000). The acceleration solver was used as the numerical flood plain solver (Bates et al., 2010). It simplifies the shallow-water

135 equations by neglecting the convective acceleration terms. This floodplain solver is usually recommended for coastal modelling and was shown to perform as well as solvers integrating the full shallow water equations with the advantage of keeping the computational time reasonable (Bates et al., 2010; Neal et al., 2012; Shaw et al., 2021). The flood maps were created using a grid resolution of $100\ m$. Elevation data was interpolated from the DEM data, and spatially varying friction grids were derived from the LU/LC Coastal Zone 2018 layer by associating each class with a literature-based Manning's coefficient (Chow, 1959;

140 Papaioannou et al., 2018). This configuration was identical for all models and was supported by model configuration sensitivity. TWL time-series were imposed as boundary conditions at the coastline of the flood model. The coastline was identified by the DEM data and the TWLs were directly interpolated from ocean model data using a nearest point method, see Section 3.3. The outputs of interest of the model are the Maximum Flooded Area (M.F.A.) extension with the maximum water depth and velocity. They will be referred to hereafter as the flood maps.

145 ### 3.2 Validation of the flood model

To assess the accuracy of the flood method and configuration applied to generate the ECFAS catalogue, flood models were developed for the twelve test cases (Section 2.4) using the real TWL time-series to force the flood model. The TWL time-series were extracted from the ECFAS hindcast (as detailed in Section 2.3) with the exception of the test cases covering the Gloria storm (2020, not included in the ECFAS hindcast) for which they were taken from the CMEMS models (Clementi et al., 2021;

150 Korres et al., 2021). The resulting flood maps were compared to the satellite-based flood maps by using three different skill indexes based on pixel comparison as suggested by Bates and De Roo (2000) and Alfieri et al. (2014) originally for fluvial events and adapted by Bates et al. (2005) and Vousdoukas et al. (2016) for coastal areas:

$$\text{H} = 100 \times \frac{F_m \cap F_o}{F_o}, \tag{2}$$

$$\text{F} = 100 \times \frac{F_m \setminus F_o}{F_o}, \tag{3}$$

155 $$\text{C} = 100 \times \frac{F_m \cap F_o}{F_m \cup F_o}, \tag{4}$$

with Fm the modelled flood and Fo the observed flood. The hit ratio H corresponds to the percentage of pixels that were flooded both in the observed and the modelled flood maps. The higher H is, the more the model floods observed flooded areas. A hit ratio of $100\ \%$ means that the flood model covered all the observed flooded areas. The false ratio F indicates the amount of false flood, calculating the number of pixels flooded by the model but not observed relative to the total number of observed flooded

160 pixels: $0\ \%$ means that the flood models did not flood more area than the observed flood. Finally, the global score C gives the

global agreement between the model and the observation, the closer it is to 100 %, the closer is the model's prediction to the observations.

To note that, the satellite image analysis detects every type of water residual, without differentiating the origin of the water surface. Thus, the observed flood map also included fluvial flooding or rain residuals if existing. As the flood model considered

165 only coastal flooding, there was a need of filtering the observed flood to obtain a fair comparison. A differentiation criterion was applied based on ground elevation: if a water surface was detected on a ground higher than the maximum TWL of the event + 1m, it was considered as non-coastal floodwater and thus discarded. In addition, for sake of consistency with the reference water surface data used to generate the observed data (Section 2.4), the flooded pixels falling into inter-tidal flats or salt marshes, as defined by the LU/LC Coastal Zone 2018 layer, were discarded.

170 Concerning the validation by comparison with the in situ flood markers, a hit ratio H_m was defined: if the model flooded the cell enclosing the marker, it was considered a hit, otherwise it was a miss. If the marker feature is a line or a polygon, and at least one of the enclosed cells was flooded, it counted as a hit. In the end, the hit ratio H_m was defined as the number of markers that were hit compared to the total number of markers available for the test case.

3.3 ECFAS catalogue

175 The ECFAS flood catalogue is a collection of flood maps gathering maximum water depth and velocity in the Maximum Flooded Area (M.F.A.). However, in the present work, only the M.F.A. will be discussed. The European coast was divided into 528 segments of 100 km length covering more than 95 % of the European coast. Then coastal sectors were defined from each coastal segment as a rectangular domain starting and ending at the extremities of the segment. The catalogue was built upon the flood modelling conducted for these 528 coastal sectors.

180 It is assumed that this collection could represent all possible short-medium return period flood scenarios affecting European coastal areas. In cases where long hindcasts or observed forcings are available, real events can be used to cover the scenarios. However, in most of the cases the real events are not sufficient, and therefore synthetic scenarios that can be defined by nearshore forcing conditions are used to cover all possible occurrences (e.g. Sanuy et al. 2018). The synthetic scenarios of the ECFAS catalogue were based on the combination of representative TWLs and storm durations derived from the ECFAS

185 hindcast (Melet et al., 2021; Montes Pérez et al., 2022). Five reference values of the forcing TWL scenarios, indexed from 1 to 5 (named L1, L2,.. L5), were defined based on the extreme values corresponding to the 2, 20 and 50 year return levels following the scheme in Table 2. This choice was determined by the need to increase the representativeness of low-medium intensity events, and to limit the uncertainty of the higher return period values estimated by the Extreme Value Analysis (EVA) performed on the ECFAS Hindcast, which only covers 10 years (see Section 2.3). The EVA was performed using the

190 methodology proposed by Mentaschi et al. (2016), employing the 97th percentile as TWL threshold of the dataset, and a declustering criteria of 72 hours for the Peak-Over-Threshold analysis (Montes Pérez et al., 2022).

Three storm durations (D): 12, 24 and 36h were used. These values were chosen based on an analysis of storm durations for all European coasts (Montes Pérez et al., 2022). The analysis was implemented by identifying coastal storms start and end times following the definitions by Harley (2017), using different sets of thresholds and meteorological independence criteria. Thus,

Reference levels L	1	2	3	4	5
TWL peak	RL2	RL2+Δ	RL2+2 × Δ	RL20	RL50

Table 2. Correspondence between TWL peak and reference level (L) results from the EVA. Δ is defined as a third of the range RL2-RL20: $\Delta = \frac{RL20-RL2}{3}$.

195   15 scenarios were designed, representing the permutation of the 5 TWL peaks and 3 durations. Hereafter, each scenario will be referred following the TWL reference index L and the storm duration D, such as L1D12 corresponds to the synthetic scenario with the first TWL reference level (2 year return period) and a 12h storm duration.

From the synthetic scenarios, synthetic storms and associated TWL time series were defined. The use of synthetic storms is common practice for storm impact assessment and counter-balances lack of observed time-series (McCall et al., 2010; Santos

200   et al., 2019; Athanasiou et al., 2021). This type of surrogate has already been suggested for coastal hazard and risk assessment (Poelhekke et al., 2016; Plomaritis et al., 2018; Sanuy et al., 2018). For this study and as illustrated in Figure 2, the shape of the temporal evolution of the storm was assumed to follow a symmetric triangle above a level identified as the "duration threshold", defined following the duration analysis mentioned above. Six-hour spin-up and spin-down times were added at the beginning and the end of the simulation to reach the duration threshold from $0\ m$ and return. The parameters, TWL peak and storm
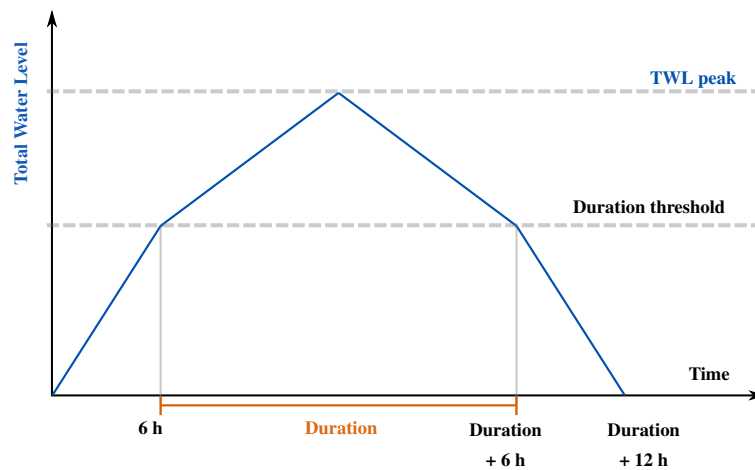
Figure 2. Definition of the synthetic storm used for forcing the flood model. TWL peaks and Durations were derived from the Extreme Value Analysis results and Duration analysis.

205   duration, were defined at each coastal point of the ECFAS combined hindcast grid with a $2.5\ km$ resolution. As the boundary conditions of the flood model were applied at the mesh coastline with a 100 m resolution, the parameters were interpolated using the nearest neighbour method. For each coastal sector, flood models were developed for each of the 15 defined scenarios leading to 15 flood maps per coastal sector.

3.4 Evaluation of the ECFAS catalogue representativeness

210 To assess the capacity of the catalogue to represent real events, and thus to validate the approximation of the total water level by the defined synthetic storms, the M.F.A. simulated by models forced by real and synthetic storm time-series were compared. Five events were considered: Xynthia at La Faute-sur-Mer (FR, 2010), Xaver at Norfolk (UK, 2013), Saint-Agatha and Vaia at Lido Delle Nazioni (IT, 2014 and 2018), and Emma at Cadiz (ES, 2018). To generate the synthetic maps, the closest synthetic storm (as defined in Section 3.3) to the real time-series were selected to force the model. The same skill scores (C, H, F

215 described in Paragraph 3.2) estimated for the validation against satellite derived flood maps were used by taking as reference the flood model from the real time-series forcing.

3.5 Assessment of flood patterns across Europe and connections to LU/LC environments

For each scenario and coastal sector, the surface of the M.F.A. was estimated from the ECFAS catalogue. Their differences between the scenarios show the sensitivity of the concerned coastal sector to the TWL peak or duration changes, and therefore

220 allow the identification of patterns along the European coasts. Considering the relative change in the M.F.A. between the peak level 1 and 5 for a 24h storm duration, normalised by the relative increase between the average peak of the TWL, the ratio α was defined as :

$$\alpha = \frac{MFA_{L5D24} - MFA_{L1D24}}{MFA_{L1D24}} \times \overline{\frac{TWL\,peak_{L1}}{TWL\,peak_{L5} - TWL\,peak_{L1}}}. \tag{5}$$

A α higher than 100 % means that the maximum flooded area increased more than the water level, while for values smaller

225 than 100 %, the flood extent did not increase as much as the water level peak.

In order to connect the flood pattern and sensitivity with LU/LC environments, the flood maps were overlaid on the LU/LC Coastal Zone 2018 data, and a relative distribution of the LU/LC first class environments inside the flooded area was estimated for each coastal sector.

4 Results

230 4.1 Validation against observed data

By direct comparison between the modelled and satellite-based maps (Figure 3 and Table 3), the flood model over-predicted the flooded area as eight test cases have a F > 100 %, and four above 1000 %. The global score C are low, from 0 to 47 %, but H score are high: half of the test cases have H > 80 %, see Figure 3 and Table 3. The best score C is reached for the test case at the Ebro Delta during the Gloria storm (2020), C = 47.67 %, while a null C is estimated for the model at Rimini during

235 Saint-Agatha (2015). The best hit score is obtained for the test case at Norfolk during Xaver (2013), H = 99.75 %, and the worst again at Rimini during Saint-Agatha (2015), H = 0 %.

Concerning the comparison with the flood markers (Table 3), five test cases out of ten have a marker hit score H_m of 100 %
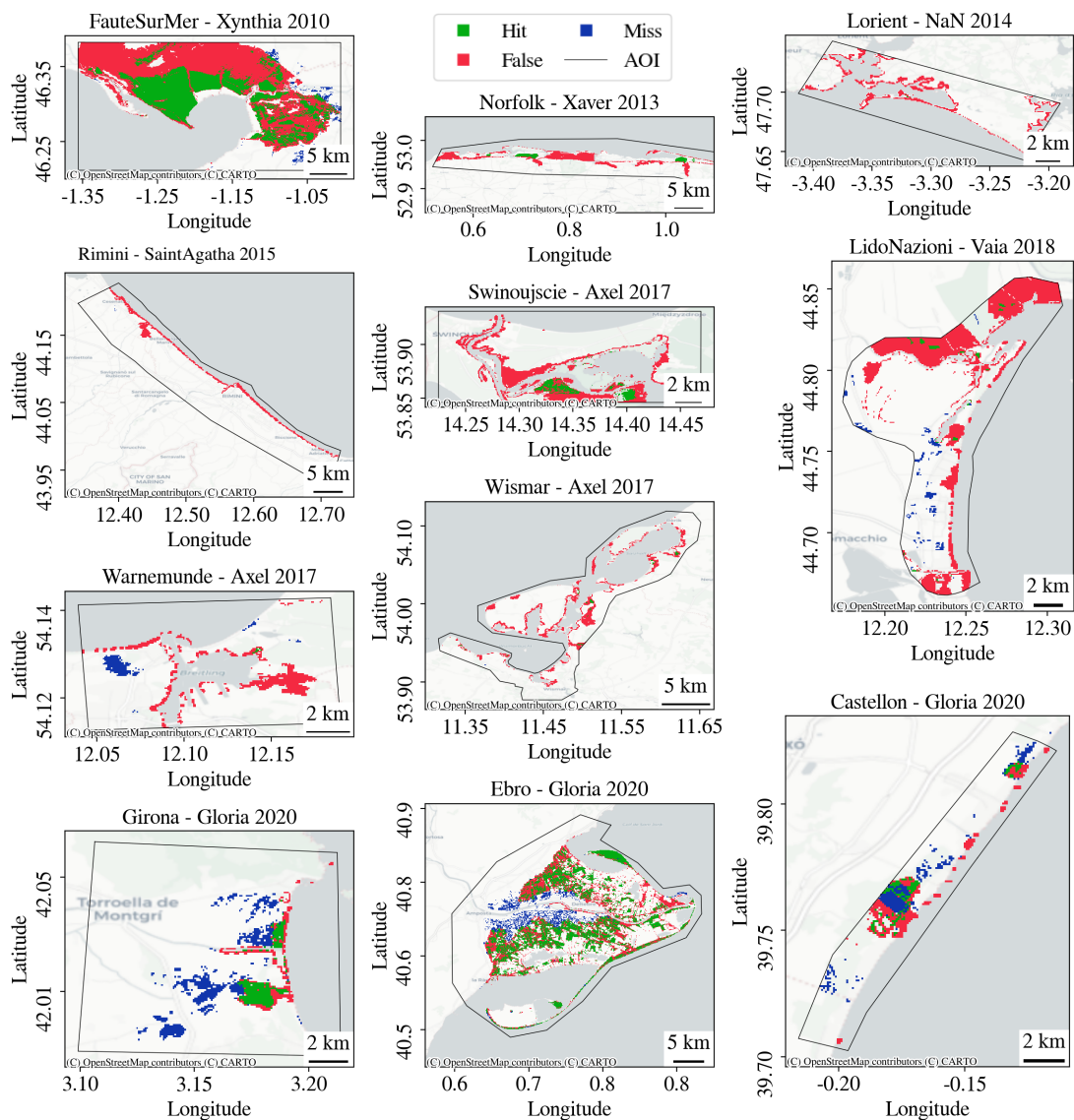
Figure 3. Performance of the model for each test case. The green areas match the intersection of the satellite-based and modelled flood (H), the blue represents the missed flood of the modelled flood, and the red areas are the flooded areas predicted by the model but not in the satellite-based flood (F). The black polygons correspond to the Area of Interest (AoI) that was defined to extract the satellite-based data. The background maps were generated using the OpenStreetMap database available through Python (Open Database License).

and one at 94.11 %. Only three test cases flooded less than half of the markers, and only the test case at Castellon during Gloria (2020) hit none of them.

Test case's name	Satellite-based flood maps			Marker points
	C [%]	H [%]	F [%]	H_m [%]
La Faute-sur-Mer - Xynthia 2010	36.07	93.49	159.15	100.00
Norfolk - Xaver 2013	11.74	99.75	749.62	100.00
Lorient - NaN 2014	0.40	85.71	21300.00	40.00
Rimini - Saint- Agatha 2015	0	0	23460	100.00
Warnemunde - Axel 2017	0.72	3.73	412.00	x
Wismar - Axel 2017	3.41	98.44	2784.49	25.00
Swijnouscie - Axel 2017	12.67	100.00	387.48	x
Cadiz - Emma 2018	x	x	x	94.11
Lido Delle Nazioni - Vaia 2018	2.30	26.74	1067.75	100
Castellon - Gloria 2020	17.58	32.7	86.04	0.00
Ebro - Gloria 2020	47.67	80.65	69.16	100.00
Girona - Gloria 2020	23.84	31.5	32.44	50.00

Table 3. Flood model skill scores (C, H, F, H_m) for each test case in comparison to observed data. x means that there is no reference data to estimate the score.

4.2 Assessment of the catalogue representativeness

To assess the capacity of the catalogue to represent real events, the flood maps of the closest TWL synthetic scenario from the catalogue were compared to those generated by the flood models forced by water level time-series extracted from the ECFAS hindcast (Section 2.3). The global scores C are above 70 %, with a hit score H larger than 90 % and a false score between 10 and 40 %, see Table 4. Even if the maps derived from the synthetic storms seem to miss some relatively small areas, particularly at Lido Delle Nazioni (not shown), they tend to slightly overpredict the flood extent, especially at La Faute-sur-Mer and Cadiz, for which the F ratios are 36 % and 22 % respectively.

Test case's name	C [%]	H [%]	F [%]
La Faute-sur-Mer Xynthia 2010	70	95	36
Norfolk - Xaver 2013	81	90	11
Lido Delle Nazioni - Saint Agatha 2015	85	97	13
Cadiz - Emma 2018	74	91	22
Lido Delle Nazioni - Vaia 2018	83	94	13

Table 4. Catalogue skill scores (C, H, F) for the closest scenario in comparison to real time-series models.

4.3 Flood spatial variability from ECFAS catalogue

Through the different scenarios, the most affected areas are on the continental North Sea coast (from Netherland to Denmark) which is exposed to the highest water level peaks and where there is a high density of flood prone areas (Figure 4). In addition, other smaller areas are highlighted, especially around estuaries such as the German Bight, the Northern part of the Adriatic Sea (Po estuary), the Gironde estuary (FR), Bristol Channel, Solway Firth and Thames estuary (UK).

For all coastal sectors, the maximum flood extent increases along with the reference level and duration. The accumulated total flood extent for the whole zone varied between 45.2 and 72.2 thousand km^2 for the weakest (L1D12) and strongest (L5D36) scenarios, respectively.

255   It is also interesting to note that the different coastal sectors do not evolve similarly with the change of the water level and storm duration (Figure 5). Indeed, the increase of the duration from 12h to 36h especially impact the Dutch coast, the Elbe and Gironde estuaries and Swimoujscie's area (Poland) with flood extent increasing more than 100 %. In addition, a few coastal sectors encapsulating estuaries: the Po, Rhone, and the central coast of Portugal (englobing the Mondego estuary and Aveiro Lagoon) are also sensitive to the storm duration with an increase of ~ 50 % of the maximum flooded areas. The relative

260 influence of the TWL peak is more general, especially with a relative increase of more than 50 % along the Mediterranean coasts, and more than 100 % in some coastal sectors such as along the Malaga coast (South of Spain).

  Concerning the relative increase of M.F.A in comparison to that of the TWL peaks, α mainly varies between 50 and 150 %, with a median at ~ 102 %, meaning that half of the coastal sectors, especially along the Mediterranean shore, witnesses a larger relative increase of the flood extent in comparison to the water level (Figure 6).

265   5   Discussions and limitations

5.1   Validation of the flood modelling method and evaluation of the synthetic storm approximation

The assessment of the flood method accuracy was strongly constrained by the quality of the available data. The very low performance of most of the test cases could be due to partial observation of the flood event from the satellite images acquired afterwards (Tarpanelli et al., 2022). Most of the satellite images were acquired a few days after the event (from 0 to 5 days,

270 see Table 1), by which time, most of the coastal water could have already withdrawn. In addition, there are observed flooded areas that seem not related to the coastal event, especially at Girona and Wismar for which water surfaces were extracted far from the coasts. Thus, the estimation of the global score C was strongly biased by the mis-representation of coastal flooding by the satellite based data. Instead, if the hit score H is considered to evaluate the model skills, the models overall performed satisfactorily with 5 test cases with H > 80 %. With the flood markers, the test cases gave, in majority, satisfactory results

275 considering that the in situ flood markers are very local data, while the methodology used for the test cases was configured for large scale. While using the hit scores to evaluate the performance of the flood model tended to favour over-prediction, it was assumed that the selected flood method correctly represented the flood process.

Concerning the comparison between real and synthetic storm time series, the synthetic storm maps accurately approximated the flood maps derived from real time-series. This confirmed the robustness of synthetic storm approximation for the selected

280 events. However, this accuracy is bound to the events that were simulated, as the triangular symmetrical shape used for the synthetic storm may not be a good representation of real storms in other locations (Duo et al., 2020). Nonetheless, the list of test cases gathered various morphologies and oceanographic conditions (on the Atlantic coast, in the North and Adriatic Seas), it was then accepted that this result can be extrapolated at European scale, and that the synthetic storms defined to generate the ECFAS flood catalogue were suitable approximations.
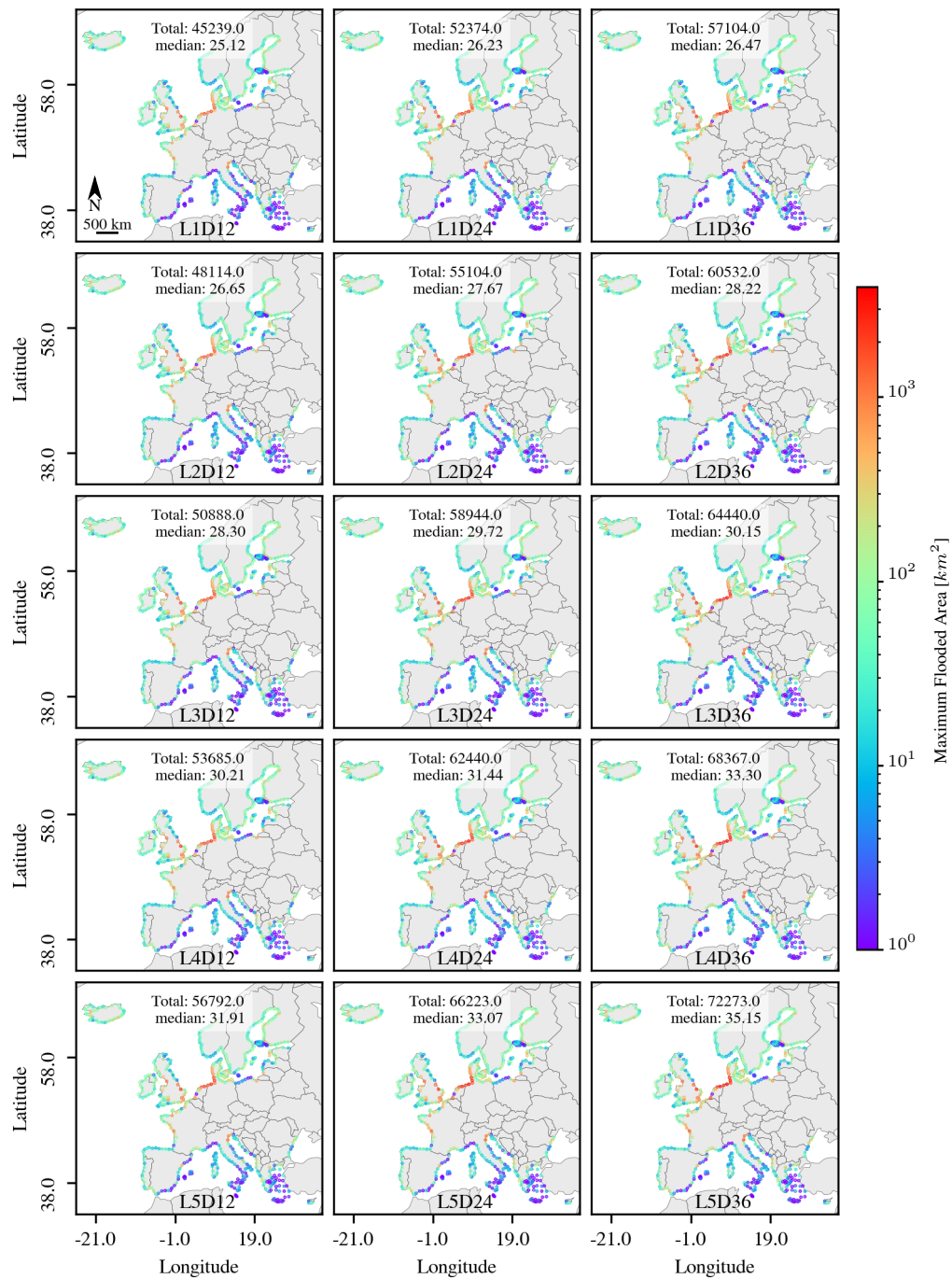
Figure 4. Maximum flooded areas for each coastal sector in km^2.
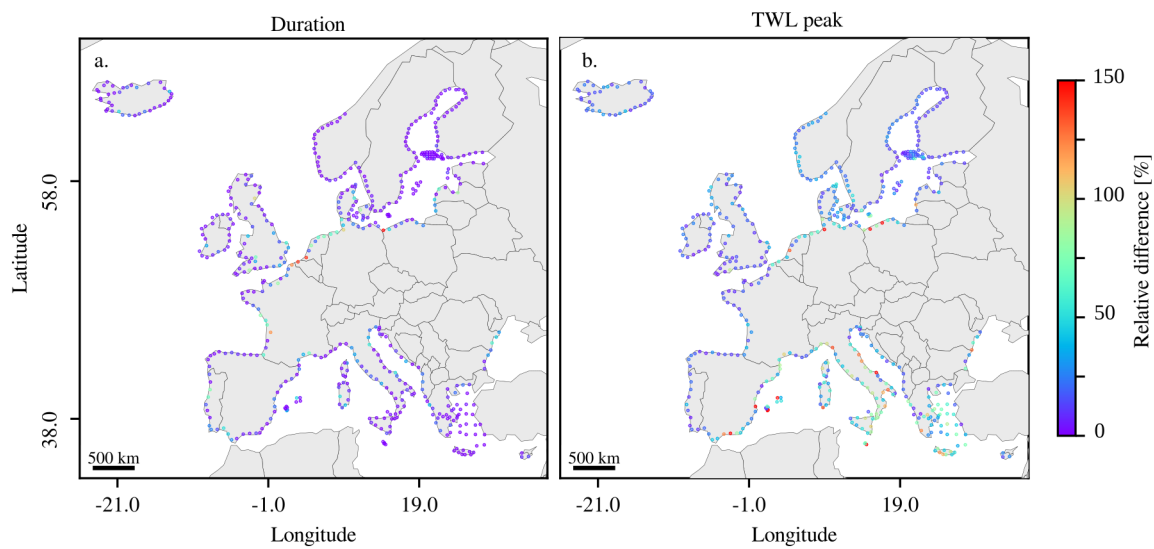
Figure 5. Maps of relative M.F.A. differences between the synthetic storm L4D36 and L4D12 scenarios (a.) and between L1D24 and L5D24 scenarios (b.).
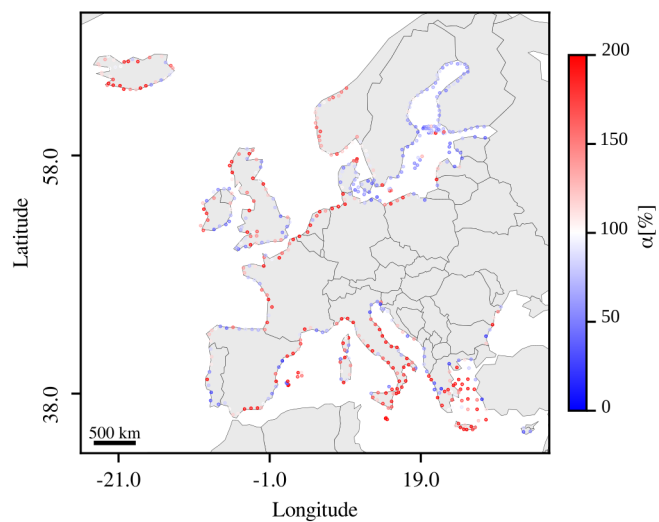
Figure 6. Maps representing the M.F.A. relative increase compared to that of TWL peaks (α) between the L1D24 and L5D24 scenarios.

5.2 Flood spatial variability from ECFAS catalogue and connection to LU/LC data

The highlighted areas exposed to the larger flood extents (Figure 4) are similar to those identified by Vousdoukas et al. (2016)
and Paprotny et al. (2019). The largest floods are correlated with flood-prone areas such as well-known low lying areas (Dutch
coast) and wetlands. Considering the relative distribution per coastal sector of the LU/LC data, as defined by the first level class
of the Coastal Zone 2018 (see nomenclature in Innerbichler et al. 2021), the maximum flooded area increases with wetland
and cropland areas (Figure 7). At the same time, coastal areas with important urban areas and open space with little vegetation,
among beaches and dunes, are those that witness the smallest floods.

The models of Vousdoukas et al. (2016) and Paprotny et al. (2019) were forced by synthetic storms corresponding to a return
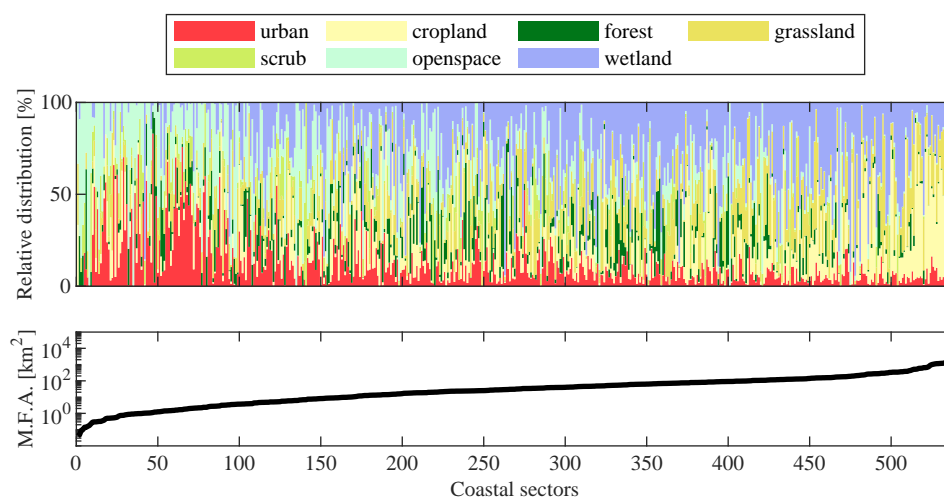
Figure 7. Relative distribution of the first level land use and land cover classes as defined by the LU/LC Coastal Zone 2018 database
(Innerbichler et al., 2021) in the flooded area for each coastal sector (upper figure). The coastal sectors are sorted by ascending maximum
flooded area for the synthetic scenario L4D24 (bottom figure).

level of 100 years with durations varying with the coastal sector. Voudouska et al. obtained a total flood extent of ∼32.5
thousand km^2, significantly smaller than any of the present total estimations for the largest peak scenario (*i.e.* matching the 50
year return level). This important discrepancy can be explained, in addition to the model configuration differences (synthetic
storm shape, DEM, etc.), by the fact that the coastal defenses were not included in the present work, and the most exposed
areas (from Netherland to Denmark) have the highest protection in Europe (∼15 m as design total water levels, see Vousdoukas
et al. 2016). This represents a limitation of the current estimation of flooded areas since only features appearing in the 10 m
DEM, downscaled at 100 m, are represented in the model grids.

Concerning the relative increase of M.F.A. compared to that of TWL peaks, α, globally, no regional trend can be identified
(Figure 6). However, the flooding of the coastal sectors in the Baltic Sea seems little sensitive to the increase of the water level
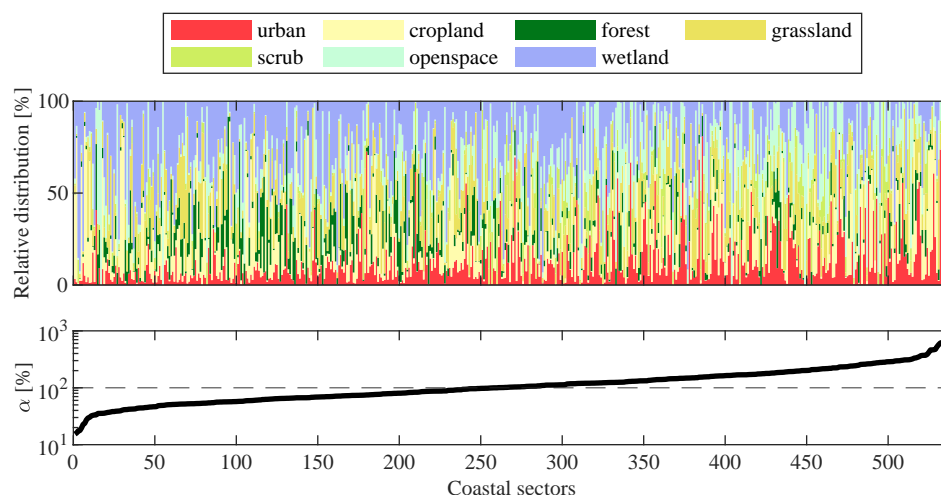
Figure 8. Relative distribution of the first level land use and land cover classes as defined by the LU/LC Coastal Zone 2018 database (Innerbichler et al., 2021) in the flooded area for each coastal sector. The coastal sectors were sorted by ascending α, being the relative difference of the maximum flooded areas compared to the relative TWL peak increase between scenarios L5 and L1 for the storm duration 24h.

peak while the Mediterranean predictions are. The coastal sectors with high α are similar to those sensitive to the increase of the water level in Figure 5b. Similarly to the M.F.A., the distribution of the LU/LC in the flooded area depending on α could indicate environments that mitigate flood spread and act as buffer zones for coastal flooding, see Figure 8. Qualitatively,

305 urban areas are more sensitive than coastal sectors with large flooded wetland surfaces. A few coastal sectors present very high α due to very small or null flooded areas for the reference scenario. These outliers were identified through the Median Absolute Deviation (M.A.D.) method and excluded for the following analysis. The evolution of the median of α, every 5 %, depending on the wetland and urban relative presence in the M.F.A show negative and positive trends, see Figure 9. This is confirmed by a significant correlation of ~ -0.29 ($p \sim 10^{-11}$) and of $\sim +0.27$ ($p \sim 10^{-10}$) between α and the wetland and

310 urban distributions, respectively. The wetland and urban areas differ in the model by the local topography and slope, and also by the Manning's friction coefficient that is imposed, as stated in Section 2.2. The identified urban areas have a Manning's coefficient of $0.013\ s.m^{-1/3}$ while those of wetland of $0.04\ s.m^{-1/3}$. Thus the friction is stronger in wetlands than in urban areas. Hence, considering friction alone, water propagation will spread more easily in urban areas once reached. Coastal flood mitigation by wetlands has already been highlighted numerous times and reviewed by Leonardi et al. (2018). Thus, the present

315 catalogue brings a global European perspective to this matter that was usually studied at local or regional scale (Smolders et al., 2015; Stark et al., 2015, 2016). From a global perspective, Van Coppenolle and Temmerman (2020) identified the Wash Bay (UK) and the Elbe Estuary as two major hot-spots in Europe where the coastlines benefit from wetland's mitigation. In the present study, α was estimated ~ 40 % at the Wash Bay, also showing a low sensitivity to the water level increase. However,

α was estimated higher than 300 % for the coastal sector with the Elbe Estuary. This could be due to the dynamic of the
river (Winterwerp et al., 2013) channeling the flood propagation that is not considered by Van Coppenolle and Temmerman
(2020), and the partial representation of the wetland due to the coastline approximation in the present model. Indeed, with
the current set up and the approximation of the boundary position, tidal flats are modelled by the combined hindcast with a
2.5 km resolution, which is not sufficient to fully represent this local complex dynamic, see Section 5.3 for the limitations of
the ECFAS catalogue.
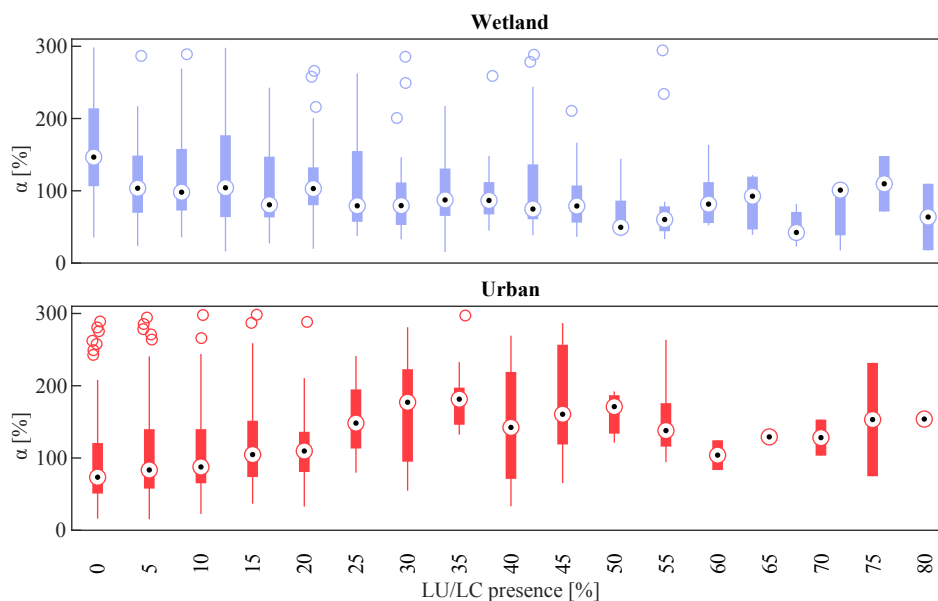
Figure 9. Evolution of α depending on the relative presence of wetland and urban environment in the maximum flooded areas of the
scenario L5D24 for each coastal sector. The black dot, thick line, thin line, single circles represent the median, the $25^{th}/75^{th}$ percentiles,
the minimum/maximum and outliers for every 5 % bin, respectively.

5.3 Limitations of the ECFAS catalogue

The development of the ECFAS flood map catalogue resulted from a balance between accuracy and computational feasibility
(Paprotny et al., 2019) to provide large-scale coastal flood assessment for European coasts. While the general method was
supported by validations, some approximations could limit the correctness of the present study. First, the flood extent estimation
is limited by the quality of the input data, such as the DEM, with a resolution of 10 m, that was coarsened to 100 m in the
modelling set up. This leads to a loss of local topography representation and may flatten out local higher ground or coastal
defenses. Therefore, the flood in some areas, such as along the Dutch coast, could be over-predicted. In addition, no man-made
flood protection structures were integrated from specific databases (Vousdoukas et al., 2016), meaning that only those detected
from the satellite images and, therefore, included in the DEM were considered.

Another major limitation is in the approximation of the boundary position, which is directly derived from the numerical grid,
335 and, therefore, the DEM and water body mask files. This led to two identified issues. Firstly, the boundary position is static, not considering morphodynamic processes such as erosion that could affect the entity of the forcing. The erosion of the beach profile has a positive feedback on the water volume entering the hinterland and should be taken into account for coastal flood modelling even for regional scale studies (Viavattene et al., 2018). Secondly, the forcing is applied at the mouth of estuaries, where interaction between estuarine circulation and incoming waves is not accounted for. Indeed, in the present configuration,
340 the flood model does not integrate the river dynamics and even the tides are schematised in a rough way, given the resolution of the global bathymetry. The model uses the acceleration flood-plain solver, only partially solving the Shallow Water equations, to propagate the surge inside the river mouth. It is then expected that the inundation propagation is not well represented in such areas. However, to take these aspects into account, more detailed datasets and local approaches, such as surge coastal propagation, are needed.

345 Concerning the catalogue scenarios, they are based on return water levels and storm durations derived from extreme value and duration analyses applied on the ECFAS combined hindcast. However, this hindcast considered only a decade of data reconstructing the TWL by linear addition of its components, excluding the run-up component, and discarding non-linear interactions with a model resolution of $2.5\ km$ at the coast. These accumulated approximations could decrease the robustness of the identified return levels. The use of the synthetic storms also contributes to the limitations of the current model. Although
350 it represents a common practice, as pointed out in Section 3.3, the use of triangular shaped storm time series can lead to non-reliable results such as for wave-driven coastal storms in the Mediterranean as demonstrated specifically for symmetric triangular synthetic storms by Duo et al. (2020).

6 Conclusions

A Pan-European flood catalogue collecting flood maps was produced for 15 medium-high frequency synthetic scenarios with
355 representative forcing parameters for each coastal sector. The scenarios combined storm surge, wave set-up and storm duration data, adding a new dimension to the existing databases in the literature. A dynamic method was applied to model the surge propagation inland and the flood modelling method was evaluated with twelve test cases spread across Europe. While this analysis was strongly restrained by the limitation of the observed satellite-based data, biasing a global estimation of the accuracy of the models, it was found that the models quite correctly represented the observed flooded areas and markers. In addition, the
360 approximation of water level real-time series using synthetic storms was proven satisfactory by comparing flood maps from the closest synthetic scenario with those based on real-time series for five events/sites.

At European level, most of the flooded area concentrated on the North Sea and additional singular locations that were connected to flood prone configurations, regardless of the TWL peak and storm duration. As the present analysis does not integrate any coastal defense, with the exception of those included in the DEM, the present estimation could be over-predicted.

365 The results across the synthetic scenarios showed different sensitivity to the increase of the water level and of the duration. While the duration mainly influences the areas identified with large flooded areas, the TWL peak is particularly impactful on

the Mediterranean coasts. In addition, most of the coastal sectors, except those in the Baltic Sea, witnessed a relatively larger increase of the flooded areas than the water level, meaning that every small water level rise could lead to more dramatic flooding. In this regard, it was found that wetlands tend to reduce this sensitivity and mitigate the flood spread while the coastal
370   sectors with larger flooded urban areas are subjected to higher flooding increase with the TWL peak.

The identified limitations of the ECFAS catalogue were mainly correlated to the quality of the input data and the approximations driven by the need to balance between accuracy and computational feasibility. This mainly concerned the missing coastal defenses and the approximation of the forcing conditions at the coastlines. Therefore, the ECFAS catalogue does not pretend to replace any local or national flood hazard estimation. Nonetheless, considering the lack of global flood hazard assessment
375   targeting high frequency (low to medium intensity) events at European scale, the present flood map catalogue fills this gap and permits an assessment of the potentially frequent coastal flood hazards along European coasts. In this way, it could be used in the prevention phase to analyse scenarios and disaster risk reduction strategies, or during preparedness phases, supporting EWS along with an operational forecasting system for nearshore forcings as proposed by the ECFAS project.

Data availability.   The ECFAS flood map catalogue is available on the Zenodo platform at the link below: Le Gal, M., Fernández Montblanc,
380   T., Montes Pérez, J., Duo, E., Souto Ceccon, P.E., Cabrita, P., & Ciavola, P. (2022). ECFAS Pan-EU Flood Catalogue, D5.4 – Pan-EU flood maps catalogue - ECFAS project (GA 101004211), https://www.ecfas.eu/ (1.3) [Data set]. Zenodo. https://doi.org/10.5281/zenodo.7488978.

Author contributions.   Marine Le Gal: Conceptualisation, Methodology, Software, Validation, Formal analysis, Investigation, Writing - Original Draft. Tomás Fernández Montblanc: Conceptualisation, Methodology, Software, Validation, Formal analysis, Investigation, Writing - Review & Editing, Supervision. Juan Montes Perez: Conceptualisation, Methodology, Software, Validation, Resources, Writing - Review &
385   Editing. Enrico Duo: Conceptualisation, Methodology, Software, Validation, Resources, Writing - Review & Editing. Vera Gastal: Methodology, Software, Validation, Resources, Writing - Review & Editing. Paulo Cabrita: Validating. Paola Souto Ceccon: Software. Paolo Ciavola: Conceptualisation, Writing - Review & Editing, Supervision. Clara Armaroli: Conceptualisation, Funding acquisition, Writing - Review & Editing.

Competing interests.   There is no competing interests.

390   *Acknowledgements.*   This work was performed within the framework of the ECFAS (A proof-of-concept for the implementation of a European Copernicus Coastal Flood Awareness System) project. ECFAS has received funding from the EU H2020 research and innovation program under Grant Agreement No 101004211. Marine Le Gal also benefited from the "Go for IT" grant (Area 04 – Scienze della Terra) from the Fondazione CRUI under the responsibility of Prof. CIAVOLA Paolo. J. Montes holds a Margarita Salas postdoctoral fellowship at the University of Cadiz from the Ministry of Universities of Spain, funded by the European Union-NextGenerationEU.

References

Alfieri, L., Salamon, P., Bianchi, A., Neal, J., Bates, P., and Feyen, L.: Advances in Pan-European Flood Hazard Mapping: Advances in Pan-European Flood Hazard Mapping, Hydrol. Process., 28, 4067–4077, https://doi.org/10.1002/hyp.9947, 2014.

Alves, B., Schiavon, E., Armaroli, C., and Velegrakis, A.: Report on the Users'Requirements, Deliverable 2.3 - ECFAS project (GA-101004211), www.ecfas.eu, 2022.

Athanasiou, P., van Dongeren, A., Giardino, A., Vousdoukas, M., Antolinez, J. A. A., and Ranasinghe, R.: A Clustering Approach for Predicting Dune Morphodynamic Response to Storms Using Typological Coastal Profiles: A Case Study at the Dutch Coast, Front. Mar. Sci., 8, 747 754, https://doi.org/10.3389/fmars.2021.747754, 2021.

Barnard, P. L., van Ormondt, M., Erikson, L. H., Eshleman, J., Hapke, C., Ruggiero, P., Adams, P. N., and Foxgrover, A. C.: Development of the Coastal Storm Modeling System (CoSMoS) for Predicting the Impact of Storms on High-Energy, Active-Margin Coasts, Nat Hazards, 74, 1095–1125, https://doi.org/10.1007/s11069-014-1236-y, 2014.

Bates, P. and De Roo, A.: A Simple Raster-Based Model for Flood Inundation Simulation, Journal of Hydrology, 236, 54–77, https://doi.org/10.1016/S0022-1694(00)00278-X, 2000.

Bates, P. D., Dawson, R. J., Hall, J. W., Horritt, M. S., Nicholls, R. J., Wicks, J., and Hassan,Mohamed: Simplified Two-Dimensional Numerical Modelling of Coastal Flooding and Example Applications, Coastal Engineering, 52, 793–810, https://doi.org/10.1016/j.coastaleng.2005.06.001, 2005.

Bates, P. D., Horritt, M. S., and Fewtrell, T. J.: A Simple Inertial Formulation of the Shallow Water Equations for Efficient Two-Dimensional Flood Inundation Modelling, Journal of Hydrology, 387, 33–45, https://doi.org/10.1016/j.jhydrol.2010.03.027, 2010.

Bates, P. D., Quinn, N., Sampson, C., Smith, A., Wing, O., Sosa, J., Savage, J., Olcese, G., Neal, J., Schumann, G., Giustarini, L., Coxon, G., Porter, J. R., Amodeo, M. F., Chu, Z., Lewis-Gruss, S., Freeman, N. B., Houser, T., Delgado, M., Hamidi, A., Bolliger, I., McCusker, K., Emanuel, K., Ferreira, C. M., Khalid, A., Haigh, I. D., Couasnon, A., Kopp, R., Hsiang, S., and Krajewski, W. F.: Combined Modeling of US Fluvial, Pluvial, and Coastal Flood Hazard Under Current and Future Climates, Water Res., 57, https://doi.org/10.1029/2020WR028673, 2021.

Calafat, F. M., Wahl, T., Tadesse, M. G., and Sparrow, S. N.: Trends in Europe Storm Surge Extremes Match the Rate of Sea-Level Rise, Nature, 603, 841–845, https://doi.org/10.1038/s41586-022-04426-5, 2022.

Chow, V. T.: Open-Channel Hydraulics, McGraw-Hill: New York, p. 728, 1959.

Clementi, E., Aydogdu, A., Goglio, A. C., Pistoia, J., Escudier, R., Drudi, M., Grandi, A., Mariani, A., Lyubartsev, V., Lecci, R., Cretí, S., Coppini, G., Masina, S., and Pinardi, N.: Mediterranean Sea Physical Analysis and Forecast (CMEMS MED-Currents, EAS6 System): MEDSEA_ANALYSISFORECAST_PHY_006_013, https://doi.org/10.25423/CMCC/MEDSEA_ANALYSISFORECAST_PHY_006_013_EAS6, 2021.

Dodet, G., Melet, A., Ardhuin, F., Bertin, X., Idier, D., and Almar, R.: The Contribution of Wind-Generated Waves to Coastal Sea-Level Changes, Surv Geophys, 40, 1563–1601, https://doi.org/10.1007/s10712-019-09557-5, 2019.

Dottori, F., Kalas, M., Salamon, P., Bianchi, A., Alfieri, L., and Feyen, L.: An Operational Procedure for Rapid Flood Risk Assessment in Europe, Nat. Hazards Earth Syst. Sci., 17, 1111–1126, https://doi.org/10.5194/nhess-17-1111-2017, 2017.

Dottori, F., Alfieri, L., Bianchi, A., Skoien, J., and Salamon, P.: A New Dataset of River Flood Hazard Maps for Europe and the Mediterranean Basin, Earth Syst. Sci. Data, 14, 1549–1569, https://doi.org/10.5194/essd-14-1549-2022, 2022.

Duo, E., Sanuy, M., Jiménez, J. A., and Ciavola, P.: How Good Are Symmetric Triangular Synthetic Storms to Represent Real Events for Coastal Hazard Modelling, Coastal Engineering, 159, 103 728, https://doi.org/10.1016/j.coastaleng.2020.103728, 2020.

European Environment Agency: Mapping the Impacts of Natural Hazards and Technological Accidents in Europe: An Overview of the Last Decade., Publications Office, LU, 2010.

435 European Space Agency and Airbus: Copernicus DEM, https://doi.org/10.5270/ESA-c5d3d65, 2022.

Fernández-Montblanc, T., Vousdoukas, M., Mentaschi, L., and Ciavola, P.: A Pan-European High Resolution Storm Surge Hindcast, Environment International, 135, 105 367, https://doi.org/10.1016/j.envint.2019.105367, 2020.

Forzieri, G., Feyen, L., Russo, S., Vousdoukas, M., Alfieri, L., Outten, S., Migliavacca, M., Bianchi, A., Rojas, R., and Cid, A.: Multi-Hazard Assessment in Europe under Climate Change, Climatic Change, 137, 105–119, https://doi.org/10.1007/s10584-016-1661-x, 2016.

440 Gallien, T., Kalligeris, N., Delisle, M.-P., Tang, B.-X., Lucey, J., and Winters, M.: Coastal Flood Modeling Challenges in Defended Urban Backshores, Geosciences, 8, 450, https://doi.org/10.3390/geosciences8120450, 2018.

Groenemeijer, P., Vajda, A., Lehtonen, I., Kämäräinen, M., Venäläinen, A., Gregow, H., and Púčik, T.: Present and Future Probability of Meteorological and Hydrological Hazards in Europe, Tech. rep., RAIN–Risk Analysis of Infrastructure Networks in Response to Extreme Weather, 2016.

445 Harley, M.: Coastal Storm Definition, in: Coastal Storms, edited by Ciavola, P. and Coco, G., pp. 1–21, John Wiley & Sons, Ltd, Chichester, UK, https://doi.org/10.1002/9781118937099.ch1, 2017.

Hersbach, H., Bell, B., Berrisford, P., Hirahara, S., Horányi, A., Muñoz-Sabater, J., Nicolas, J., Peubey, C., Radu, R., Schepers, D., Simmons, A., Soci, C., Abdalla, S., Abellan, X., Balsamo, G., Bechtold, P., Biavati, G., Bidlot, J., Bonavita, M., Chiara, G., Dahlgren, P., Dee, D., Diamantakis, M., Dragani, R., Flemming, J., Forbes, R., Fuentes, M., Geer, A., Haimberger, L., Healy, S., Hogan, R. J., Hólm, E.,

450 Janisková, M., Keeley, S., Laloyaux, P., Lopez, P., Lupu, C., Radnoti, G., Rosnay, P., Rozum, I., Vamborg, F., Villaume, S., and Thépaut, J.-N.: The ERA5 Global Reanalysis, Q.J.R. Meteorol. Soc., 146, 1999–2049, https://doi.org/10.1002/qj.3803, 2020.

Hinkel, J., Lincke, D., Vafeidis, A. T., Perrette, M., Nicholls, R. J., Tol, R. S. J., Marzeion, B., Fettweis, X., Ionescu, C., and Levermann, A.: Coastal Flood Damage and Adaptation Costs under 21st Century Sea-Level Rise, Proc. Natl. Acad. Sci. U.S.A., 111, 3292–3297, https://doi.org/10.1073/pnas.1222469111, 2014.

455 Holman, R. A. and Sallenger, A. H.: Setup and Swash on a Natural Beach, J. Geophys. Res., 90, 945, https://doi.org/10.1029/JC090iC01p00945, 1985.

Ieronymidi, E. and Grigoriadis, D.: Coastal Dataset Including Exposure and Vulnerability Layers, Deliverable 3.1 - ECFAS Project (GA 101004211), Www.Ecfas.Eu, https://doi.org/10.5281/ZENODO.7319270, 2022.

Innerbichler, F., Kreisel, A., and Gruber, C.: Coastal Zones Nomenclature Guideline, Tech. rep., Copernicus Land Monitoring Service, 2021.

460 Irazoqui Apecechea, M., Melet, A., and Armaroli, C.: Towards a Pan-European Coastal Flood Awareness System: Skill of Extreme Sea-Level Forecasts from the Copernicus Marine Service, Front. Mar. Sci., 9, 1091 844, https://doi.org/10.3389/fmars.2022.1091844, 2023.

Korres, G., Ravdas, M., Zacharioudaki, A., Denaxa, D., and Sotiropoulou, M.: Mediterranean Sea Waves Analysis and Forecast (CMEMS Med-Waves, MedWAM3 System): MEDSEA ANALYSISFORECAST WAV 006 017, https://doi.org/10.25423/CMCC/MEDSEA_ANALYSISFORECAST_WAV_006_017_MEDWAM3, 2021.

465 Lellouche, J.-M., Greiner, E., Bourdallé-Badie, R., Gilles, G., Melet, A., Drévillon, M., Bricaud, C., Hamon, M., Le Galloudec, O., Regnier, C., Candela, T., Testut, C.-E., Gasparin, F., Ruggiero, G., Benkiran, M., Drillet, Y., and Le Traon, P.-Y.: The Copernicus Global 1/12° Oceanic and Sea Ice GLORYS12 Reanalysis, Front. Earth Sci., 9, 698 876, https://doi.org/10.3389/feart.2021.698876, 2021.

Leonardi, N., Carnacina, I., Donatelli, C., Ganju, N. K., Plater, A. J., Schuerch, M., and Temmerman, S.: Dynamic Interactions between Coastal Storms and Salt Marshes: A Review, Geomorphology, 301, 92–107, https://doi.org/10.1016/j.geomorph.2017.11.001, 2018.

470 Lyard, F. H., Allain, D. J., Cancet, M., Carrère, L., and Picot, N.: FES2014 Global Ocean Tide Atlas: Design and Performance, Ocean Sci., 17, 615–649, https://doi.org/10.5194/os-17-615-2021, 2021.

McCall, R., Van Thiel de Vries, J., Plant, N., Van Dongeren, A., Roelvink, J., Thompson, D., and Reniers, A.: Two-Dimensional Time Dependent Hurricane Overwash and Erosion Modeling at Santa Rosa Island, Coastal Engineering, 57, 668–683, https://doi.org/10.1016/j.coastaleng.2010.02.006, 2010.

475 Melet, A., Meyssignac, B., Almar, R., and Le Cozannet, G.: Under-Estimated Wave Contribution to Coastal Sea-Level Rise, Nature Clim Change, 8, 234–239, https://doi.org/10.1038/s41558-018-0088-y, 2018.

Melet, A., Irazoqui Apecechea, M., Fernández-Montblanc, T., and Ciavola, P.: Report on the Calibration and Validation of Hindcasts and Forecasts of Total Water Level along European Coasts, Deliverable 4.1 - ECFAS project (GA 101004211), https://doi.org/10.5281/ZENODO.7488687, 2021.

480 Mentaschi, L., Vousdoukas, M., Voukouvalas, E., Sartini, L., Feyen, L., Besio, G., and Alfieri, L.: The Transformed-Stationary Approach: A Generic and Simplified Methodology for Non-Stationary Extreme Value Analysis, Hydrol. Earth Syst. Sci., 20, 3527–3547, https://doi.org/10.5194/hess-20-3527-2016, 2016.

Merkens, J.-L., Reimann, L., Hinkel, J., and Vafeidis, A. T.: Gridded Population Projections for the Coastal Zone under the Shared Socioeconomic Pathways, Global and Planetary Change, 145, 57–66, https://doi.org/10.1016/j.gloplacha.2016.08.009, 2016.

485 Mokrech, M., Kebede, A. S., Nicholls, R. J., Wimmer, F., and Feyen, L.: An Integrated Approach for Assessing Flood Impacts Due to Future Climate and Socio-Economic Conditions and the Scope of Adaptation in Europe, Climatic Change, 128, 245–260, https://doi.org/10.1007/s10584-014-1298-6, 2015.

Montes Pérez, J., Duo, E., and Fernández-Montblanc, T.: Report on the Identification of Local Thresholds of TWL for Triggering Coastal Flooding, Deliverable 4.3 – ECFAS project (GA 101004211), Zenodo, https://doi.org/10.5281/ZENODO.6782582, 2022.

490 Muis, S., Verlaan, M., Winsemius, H. C., Aerts, J. C. J. H., and Ward, P. J.: A Global Reanalysis of Storm Surges and Extreme Sea Levels, Nat Commun, 7, 11 969, https://doi.org/10.1038/ncomms11969, 2016.

Neal, J., Villanueva, I., Wright, N., Willis, T., Fewtrell, T., and Bates, P.: How Much Physical Complexity Is Needed to Model Flood Inundation?, Hydrol. Process., 26, 2264–2282, https://doi.org/10.1002/hyp.8339, 2012.

Papaioannou, G., Efstratiadis, A., Vasiliades, L., Loukas, A., Papalexiou, S. M., Koukouvinos, A., Tsoukalas, I., and
495 Kossieris, P.: An Operational Method for Flood Directive Implementation in Ungauged Urban Areas, Hydrology, 5, 24, https://doi.org/10.3390/hydrology5020024, 2018.

Paprotny, D., Morales-Nápoles, O., and Nikulin, G.: Extreme Sea Levels under Present and Future Climate: A Pan-European Database, E3S Web Conf., 7, 02 001, https://doi.org/10.1051/e3sconf/20160702001, 2016.

Paprotny, D., Morales-Nápoles, O., Vousdoukas, M. I., Jonkman, S. N., and Nikulin, G.: Accuracy of pan-European Coastal Flood Mapping,
500 J Flood Risk Management, 12, e12 459, https://doi.org/10.1111/jfr3.12459, 2019.

Plomaritis, T. A., Costas, S., and Ferreira, O.: Use of a Bayesian Network for Coastal Hazards, Impact and Disaster Risk Reduction Assessment at a Coastal Barrier (Ria Formosa, Portugal), Coastal Engineering, 134, 134–147, https://doi.org/10.1016/j.coastaleng.2017.07.003, 2018.

Poelhekke, L., Jäger, W. S., van Dongeren, A., Plomaritis, T. A., McCall, R., and Ferreira, O.: Predicting Coastal Hazards for Sandy Coasts
505 with a Bayesian Network, Coastal Engineering, 118, 21–34, https://doi.org/10.1016/j.coastaleng.2016.08.011, 2016.

Portner, H., Roberts, D., Tignor, M., Poloczanska, E., Mintenbeck, K., Alegria, A., Craig, M., Langsdorf, S., Loschke, S., Moller, V., Okem, A., and Rama, B.: IPCC: Climate Change 2022: Impacts, Adaptation and Vulnerability. Contribution of Working Group II to the Sixth Assessment Report of the Intergovernmental Panel on Climate Change, Tech. rep., Cambridge University Press, Cambridge, UK and New York, NY, USA,, 2022.

510 Santos, V. M., Wahl, T., Long, J. W., Passeri, D. L., and Plant, N. G.: Combining Numerical and Statistical Models to Predict Storm-Induced Dune Erosion, J. Geophys. Res. Earth Surf., 124, 1817–1834, https://doi.org/10.1029/2019JF005016, 2019.

Sanuy, M., Duo, E., Jäger, W. S., Ciavola, P., and Jiménez, J. A.: Linking Source with Consequences of Coastal Storm Impacts for Climate Change and Risk Reduction Scenarios for Mediterranean Sandy Beaches, Nat. Hazards Earth Syst. Sci., 18, 1825–1847, https://doi.org/10.5194/nhess-18-1825-2018, 2018.

515 Seenath, A., Wilson, M., and Miller, K.: Hydrodynamic versus GIS Modelling for Coastal Flood Vulnerability Assessment: Which Is Better for Guiding Coastal Management?, Ocean & Coastal Management, 120, 99–109, https://doi.org/10.1016/j.ocecoaman.2015.11.019, 2016.

Shaw, J., Kesserwani, G., Neal, J., Bates, P., and Sharifian, M. K.: LISFLOOD-FP 8.0: The New Discontinuous Galerkin Shallow-Water Solver for Multi-Core CPUs and GPUs, Geosci. Model Dev., 14, 3577–3602, https://doi.org/10.5194/gmd-14-3577-2021, 2021.

Smith, P., Pappenberger, F., Wetterhall, F., Thielen del Pozo, J., Krzeminski, B., Salamon, P., Muraro, D., Kalas, M., and Baugh, C.:
520 On the Operational Implementation of the European Flood Awareness System (EFAS), in: Flood Forecasting, pp. 313–348, Elsevier, https://doi.org/10.1016/B978-0-12-801884-2.00011-6, 2016.

Smolders, S., Plancke, Y., Ides, S., Meire, P., and Temmerman, S.: Role of Intertidal Wetlands for Tidal and Storm Tide Attenuation along a Confined Estuary: A Model Study, Preprint, Sea, Ocean and Coastal Hazards, https://doi.org/10.5194/nhessd-3-3181-2015, 2015.

Souto Ceccon, P., Duo, E., Fernandez Montblanc, T., Montes, J., Ciavola, P., and Armaroli, C.: A New European Coastal Storm Impact
525 Database of Resources: The ECFAS Effort, in: Proceedings of the 39th IAHR World Congress, pp. 6646–6652, International Association for Hydro-Environment Engineering and Research (IAHR), https://doi.org/10.3850/IAHR-39WC2521711920221117, 2022.

Stark, J., Van Oyen, T., Meire, P., and Temmerman, S.: Observations of Tidal and Storm Surge Attenuation in a Large Tidal Marsh: Tidal and Storm Surge Attenuation in a Marsh, Limnol. Oceanogr., 60, 1371–1381, https://doi.org/10.1002/lno.10104, 2015.

Stark, J., Plancke, Y., Ides, S., Meire, P., and Temmerman, S.: Coastal Flood Protection by a Combined Nature-Based and Engineer-
530 ing Approach: Modeling the Effects of Marsh Geometry and Surrounding Dikes, Estuarine, Coastal and Shelf Science, 175, 34–45, https://doi.org/10.1016/j.ecss.2016.03.027, 2016.

Tarpanelli, A., Mondini, A. C., and Camici, S.: Effectiveness of Sentinel-1 and Sentinel-2 for Flood Detection Assessment in Europe, Nat. Hazards Earth Syst. Sci., 22, 2473–2489, https://doi.org/10.5194/nhess-22-2473-2022, 2022.

U.S. Army Corps of Engineers: Coastal Engineering Manual (Cem), Washington DC, Engineer manual 1110-2-1100, 2002.

535 Vafeidis, A. T., Nicholls, R. J., McFadden, L., Tol, R. S. J., Hinkel, J., Spencer, T., Grashoff, P. S., Boot, G., and Klein, R. J. T.: A New Global Coastal Database for Impact and Vulnerability Analysis to Sea-Level Rise, Journal of Coastal Research, 244, 917–924, https://doi.org/10.2112/06-0725.1, 2008.

Van Coppenolle, R. and Temmerman, S.: Identifying Global Hotspots Where Coastal Wetland Conservation Can Contribute to Nature-Based Mitigation of Coastal Flood Risks, Global and Planetary Change, 187, 103 125, https://doi.org/10.1016/j.gloplacha.2020.103125, 2020.

540 Viavattene, C., Jiménez, J., Ferreira, O., Priest, S., Owen, D., and McCall, R.: Selecting Coastal Hotspots to Storm Impacts at the Regional Scale: A Coastal Risk Assessment Framework, Coastal Engineering, 134, 33–47, https://doi.org/10.1016/j.coastaleng.2017.09.002, 2018.

Vousdoukas, M. I., Voukouvalas, E., Mentaschi, L., Dottori, F., Giardino, A., Bouziotas, D., Bianchi, A., Salamon, P., and Feyen, L.: Developments in Large-Scale Coastal Flood Hazard Mapping, Natural Hazards and Earth System Sciences, 16, 1841–1853, https://doi.org/10.5194/nhess-16-1841-2016, 2016.

545 Wahl, T., Mudersbach, C., and Jensen, J.: Assessing the Hydrodynamic Boundary Conditions for Risk Analyses in Coastal Areas: A Stochastic Storm Surge Model, Nat. Hazards Earth Syst. Sci., 11, 2925–2939, https://doi.org/10.5194/nhess-11-2925-2011, 2011.

Winterwerp, J. C., Wang, Z. B., van Braeckel, A., van Holland, G., and Kösters, F.: Man-Induced Regime Shifts in Small Estuaries—II: A Comparison of Rivers, Ocean Dynamics, 63, 1293–1306, https://doi.org/10.1007/s10236-013-0663-8, 2013.

Xu, H.: Modification of Normalised Difference Water Index (NDWI) to Enhance Open Water Features in Remotely Sensed Imagery, International Journal of Remote Sensing, 27, 3025–3033, https://doi.org/10.1080/01431160600589179, 2006.